

# The effect of off-diagonal density matrix in DFT+DMFT for $\text{Li}_2\text{MnO}_3$

Alex Taekyung Lee and Anh T. Ngo\*

*Department of Chemical engineering, University of Illinois at Chicago, Chicago, IL 60608, USA and  
Materials Science Division, Argonne National laboratory, Lemont, IL 60439, USA*

Hyowon Park

*Department of Physics, University of Illinois at Chicago, Chicago, IL 60608, USA and  
Materials Science Division, Argonne National laboratory, Lemont, IL 60439, USA*

(Dated: April 5, 2023)

$\text{Li}_2\text{MnO}_3$  has garnered much attention as one of the new-generation battery material, due to the high capacity and low cost. In the present work, we performed density functional theory (DFT)+ $U$  and dynamical mean field theory (DMFT) calculations with continuous time quantum Monte Carlo impurity solver to study the electronic properties of  $\text{Li}_2\text{MnO}_3$ . Due to the nature of monoclinic  $C2/m$  symmetry, the off-diagonal terms in the  $d$ -orbital block Hamiltonian (and  $d$ -orbital density matrix) are large, which results the large suppression of the energy gap due to the underestimation of the crystal-field splitting. We diagonalize the Mn  $d$  block in the full  $p-d$  Hamiltonian by applying unitary rotation matrix, and obtained an energy gap of 0.8eV, although it is still smaller than the experimental gap of 2.1 eV even with the large  $U$ . In the  $p-d$  model, a small double counting energy is essential to reduce the  $p-d$  hybridization, thus to obtain the experimental gap. We show that the low-energy ( $d$ -only basis) model is efficient to study the electronic structure of  $\text{Li}_2\text{MnO}_3$ , since the Wannier basis is the hybridized state of Mn  $d$  and O  $p$  orbitals. These results suggest the correct way to investigate the low-symmetry materials using DFT+ DMFT method and to our knowledge, there is no systematic study of the effect of the off-diagonal terms so far. We also find that the antiferromagnetic ground state  $\Gamma_{2u}$  is stable with  $U \leq 2$  within DFT+ $U$ , which is much smaller than widely used  $U=5$  eV.

PACS numbers:

## I. Introduction

In the past two decades, the demand for the batteries has been enormously grown due to the advances in technology of portable devices and electric vehicles [1]. Lithium-ion battery technology has contributed greatly to this demand, and have been extensively studied. Traditional cathode materials for Li-battery is transition metal (TM) oxides with extractable Li ions, where TM atoms are  $3d$  elements Cr, Co, Ni, Fe, or Mn or  $4d$  elements Mo or Ru [2–4]. Recently,  $\text{Li}_2\text{MnO}_3$  attracted much attention as a next generation of cathode material, due to the high voltage (4.4–5 V) and the low cost [2, 5].  $\text{Li}_2\text{MnO}_3$  has a layered structure with  $C/2m$  space group (Fig. 1), and Li atoms are located between  $\text{MnO}_3$  layer and at the center of the hexagon. During the charging and discharging process of the battery, Li ions are removed or added, respectively. Therefore, studying atomic, electronic, and magnetic properties  $\text{Li}_2\text{MnO}_3$  is important to understand and improve the performance of the batteries.

$\text{Li}_2\text{MnO}_3$  is an insulator with a band gap of 2.1 [6]–2.17 [7] eV. Mn ion in  $\text{Li}_2\text{MnO}_3$  has  $4+$  charge states ( $d^3$ ), and it has high-spin configuration ( $S = 3/2$ ) with magnetic moment of 2.3–2.7  $\mu_B$  [8, 9]. In the high-spin state, 3  $d$  electrons fully occupy the spin-up  $t_{2g}$  band,

and thus  $\text{Mn}^{4+}$  has a nonzero gap due to the crystal field splitting and Hund coupling. At low temperature,  $\text{Li}_2\text{MnO}_3$  is antiferromagnetic with Néel temperature of  $T_N = 36\text{--}36.5$  K [8, 9]. While the antiferromagnetic ground state of  $\Gamma_{3g}$  is reported in early study [9], recent study suggested that  $\Gamma_{2u}$  is the ground state, while both  $\Gamma_{3g}$  and  $\Gamma_{2u}$  have same magnetic propagation vector  $Q_m = (0, 0, 0.5)$ .

There are several studies of  $\text{Li}_2\text{MnO}_3$  through the density functional theory (DFT) [2, 10–14]. However, detailed electronic and magnetic structures are not fully understood yet. While the band gaps are predicted within DFT+ $U$  [10, 11], GW calculation [2] or using hybrid functionals [2, 12], previous studies did not focus on the magnetic ground state, and only consider nonmagnetic [2, 14] or ferromagnetic [10–12] configurations. Given that the operating temperature of the battery is around room temperature and  $T_N$  of  $\text{Li}_2\text{MnO}_3$  is only 36 K [8], paramagnetic phase of  $\text{Li}_2\text{MnO}_3$  is very important. However, nonmagnetic calculation within DFT cannot describe the paramagnetic spin order properly, since the paramagnetic phase has zero averaged spin due to the fluctuations of the local spin, while there is no local spin in the nonmagnetic phase. To study the paramagnetic phase of  $\text{Li}_2\text{MnO}_3$  at finite temperature, more advanced theories such as dynamical mean field theory (DMFT) is needed.

Other transition metal oxides Li batteries, such as  $\text{LiCoO}_2$  [15] and  $\text{LiNiO}_2$  [16] are also studied within DFT+DMFT, and it has been shown that the electronic

---

\*anhngo@uic.edu

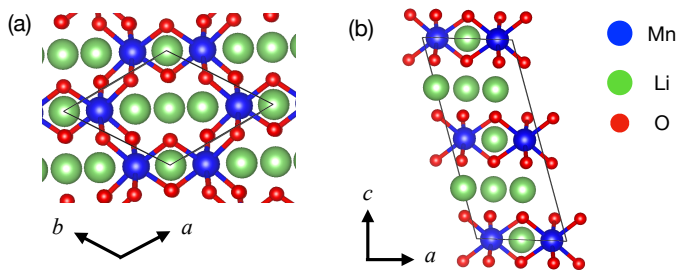


FIG. 1: (a) top and (b) side view for the atomic structure of  $\text{Li}_2\text{MnO}_3$ . Li atoms are located between  $\text{MnO}_3$  layers and the center of the hexagon.

structure and the energy gap size of  $\text{LiNiO}_2$  strongly depends on the choice of the different Wannier basis [16]. Since the symmetry of  $\text{Li}_2\text{MnO}_3$  ( $C2/m$ ), is lower than the symmetry of  $\text{LiNiO}_2$  ( $R\bar{3}m$ ), the distortion of TM-O octahedron is larger in  $\text{Li}_2\text{MnO}_3$ , and thus the choice of the Wannier basis can be even more important for  $\text{Li}_2\text{MnO}_3$ . Therefore, the systematic study of  $\text{Li}_2\text{MnO}_3$  with different basis is needed within DFT+DMFT.

In the present work, we performed DFT+DMFT calculation [17] to study the electronic structure of  $\text{Li}_2\text{MnO}_3$ .  $\text{Li}_2\text{MnO}_3$  has  $C2/m$  symmetry with the  $C_{2h}$  point group symmetry of Mn ion, and the Mn-O<sub>6</sub> octahedron is squeezed along the [111] direction (see Figure 8 in Appendix A). As a result, the Wannier Hamiltonian projected along the global coordinate has large off-diagonal terms, which result the large suppression of the energy gap within DMFT using  $U=5$ , while the off-diagonal terms are neglected in the quantum Monte Carlo impurity solver. Off-diagonal terms are reduced by using the Wannier basis close to the local coordinate of  $\text{MnO}_6$ , but they are still large and the energy gap is still suppressed, because of the local symmetry of  $\text{MnO}_6$  is  $C_{2h}$ . To reduce the effect of the off-diagonal terms, we diagonalize the block diagonal part of Mn  $d$  Hamiltonian, by applying unitary rotation matrix. Block-diagonalization of the Hamiltonian enhances the gap, but the gap is still much smaller than the experimental value, and increasing  $U$  cannot resolve the problem.

Experimental gap is obtained by using nonzero double counting term and increasing  $U$ . Since the double counting term represents the  $p-d$  covalency, importance of the double counting term indicates that  $p-d$  correlation is also important on the electronic structure of  $\text{Li}_2\text{MnO}_3$ . Finally we considered  $d$ -only model Hamiltonian for DMFT. Since the Wannier  $d$  basis of effective model is a hybridized state of Mn  $d$  and O  $p$ ,  $U$  of effective low-energy model (we refer it as  $d$ -only model) provides both  $d-d$  and  $p-d$  correlation. Therefore, the energy gap is sensitive on  $U$  with  $d$ -only model, and experimental energy gap is obtained with small  $U$  value.

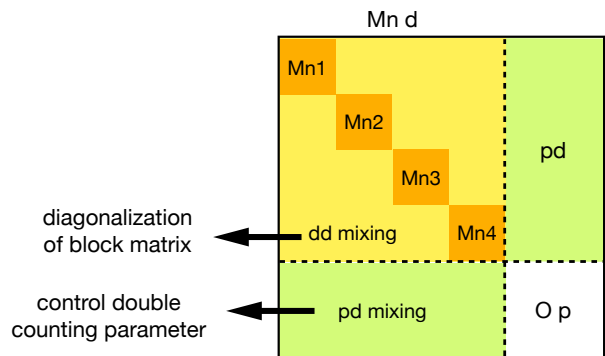


FIG. 2: Schematic diagram of the Wannier Hamiltonian matrix for Mn  $d$  and O  $p$  orbitals. We diagonalize the diagonal blocks of each Mn  $d$  states (orange boxes), and control  $p-d$  correlation by changing double counting parameter.

## II. Methods

### A. DFT+DMFT

We employ the non-charge-self-consistent DFT+DMFT method [17, 18] for relaxed structures obtained from DFT calculations. For DFT calculation, we use the projector augmented wave (PAW) method [19] and the revised version of the generalized gradient approximation (GGA) proposed by Perdew *et al.* (PBEsol) [20] as implemented in the VASP software [21]. In all cases, the spin-dependent version of the exchange correlation functional is employed. A plane wave basis with a kinetic energy cutoff of 500 eV is used. We used 24 atom unit cells (i.e.,  $1 \times 1 \times 2$  unit cells), which contains 4 Mn atoms, and  $\Gamma$ -centered  $\mathbf{k}$ -point meshes of size  $10 \times 10 \times 5$ . Atomic positions within the unit cells were relaxed until the residual forces were less than 0.01 eV/Å, and the stress was relaxed below 0.02 kB.

We solve the many-body problem on the manifold of both Mn  $3d+O p$  Wannier orbitals and Mn  $3d$ -only orbitals. The DFT+DMFT calculation has the following steps. First, we solve the non-spin-polarized Kohn-Sham (KS) equation within DFT using VASP. Second, we construct a localized-basis Hamiltonian for the Mn  $3d$  bands by generating maximally localized Wannier functions (MLWFs) [22] for the nonmagnetic DFT band structure. Finally, we solve the DMFT self-consistent equations for the correlated subspace of Mn  $3d$  and O  $p$  Wannier orbitals (or only Mn  $3d$  orbitals) using the continuous time quantum Monte Carlo (CTQMC) [23, 24] impurity solver. Both Hubbard  $U$  and Hund's couplings  $J$  are parameterized by the  $(F^0, F^2, F^4)$  Slater integrals, using  $U = F^0$  and  $J = (F^2 + F^4)/14$ . Only Coulomb interaction matrix elements of the density-density types are considered in the CTQMC while the spin-flip and pair-hopping terms are neglected. For the  $pd$  model Hamiltonian, we used  $U$  values of 5 and 7 eV and  $J$  of 0.9 eV.

We used electronic temperatures of 300 K to study the temperature effect on the spectral function.

We note that applying DMFT method to  $\text{Li}_2\text{MnO}_3$  has two issues: (i) there are large off-diagonal terms in the Wannier Hamiltonian (yellow region in Fig. 2), (ii)  $p-d$  correlation is important due to the strong  $p-d$  hybridization (green region in Fig. 2). To overcome these problems, we (i) diagonalize the block  $d$  Hamiltonian and (ii) use different values of double counting parameters, as summarized in Fig. 2.

If the off-diagonal terms in the Hamiltonian are large, they can induce large error within DMFT, since CTQMC only treat the diagonal terms of the Hamiltonian to avoid the sign problem. The cartesian axes of the Wannier orbitals and the directions of the Mn-O bonds are not parallel, due to the  $C_{2h}$  point group symmetry of  $\text{MnO}_6$  octahedron. If the point group symmetry of TM octahedron is not cubic, e.g., trigonal or monoclinic, then there is large mixing of  $d$  basis ( $d_{xy}$ ,  $d_{xz}$ ,  $d_{yz}$ ,  $d_{z^2}$ ,  $d_{x^2-y^2}$ ), since this basis is defined by the cubic crystal field. In this case, the off-diagonal terms of the Wannier Hamiltonian with cubic  $d$  orbital basis are large, and results in the error within DMFT. Note that DFT+ $U$  does not have such problem since DFT+ $U$  is rotationally invariant [25] and thus can have off-diagonal terms in the density matrix.

On the other hand, if  $p-d$  hybridization is strong as the nickelates [26, 27], applying nonzero  $U$  on  $pd$  Wannier Hamiltonian may not capture the physics of  $pd$  correlation properly. To resolve this issue, we use the double counting parameter, which control the degree of  $p-d$  covalency. In term of double counting corrections for DFT+DMFT, we use a double counting energy ( $E^{\text{DC}}$ ) and potential ( $V^{\text{DC}} = \partial E^{\text{DC}} / \partial N_d$ ) similar to the conventional fully localized limit [18, 28]:

$$E^{\text{DC}} = \frac{U}{2} N_d \cdot (N_d - 1) - \frac{J}{4} N_d \cdot (N_d - 2), \quad (1)$$

$$V^{\text{DC}} = \frac{U}{2} \left( \bar{N}_d - \frac{1}{2} \right) - \frac{J}{2} (\bar{N}_d - 1) \quad (2)$$

Here  $\bar{N}_d = N_d - \alpha$ , where  $N_d$  is the  $d$  occupancy obtained self-consistently at each Mn site, and  $\alpha$  is double counting parameter. Note that  $\alpha = 0$  gives the conventional fully localized limit. From the Eqs. 1 and 2, changing  $\alpha$  (or  $V^{\text{DC}}$ ) can tune the  $p-d$  covalency by effectively shifting the  $d$  orbital level. If  $V^{\text{DC}}$  potential is smaller than the DC potential of fully localized limit, it will make  $d$  orbital level higher and the covalency effect weaker, with reduced  $N_d$ .

### B. DFT+ $U$ and atomic structures

The GGA+ $U$  scheme within the rotationally invariant formalism together with the fully localized limit double-

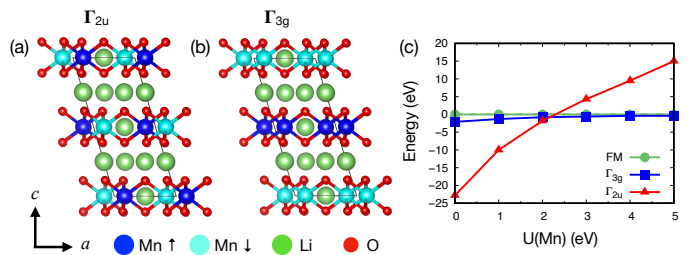


FIG. 3: Possible magnetic phases of  $\text{Li}_2\text{MnO}_3$  at low temperature, (a)  $\Gamma_{2u}$  and (b)  $\Gamma_{3g}$ . Mn ions with spin-up and spin-down are represented by different colors (blue and sky-blue). (c) the relative energies of the ferromagnetic,  $\Gamma_{2u}$ , and  $\Gamma_{3g}$  phases, as a function of  $U(\text{Mn})$ . Energy of the ferromagnetic phase is set to be zero.

counting formula [25] is used to study the effect of electron interactions. In this work, we do not employ a Hund's  $J$  parameter for any atom in our DFT+ $U$  calculations. As explained by prior work, (i) our spin-dependent PBE DFT exchange-correlation functional already describes a sizable exchange interaction prior to including of any + $U$  correction, and (ii) further inclusion of a  $J$  atop a spin-dependent functional can lead to unexpected (and/or incorrect) physical behavior in a number of transition metal oxides [26, 29, 30]. Projected density of states are obtained by the spherical harmonic projections inside spheres around each atom. Wigner-Seitz radii of 1.323 Å were used for the projection of Mn atoms, respectively, as implemented in the VASP-PAW pseudopotential.

### III. Results and discussion

There are several DFT+ $U$  studies of  $\text{Li}_2\text{MnO}_3$ , while  $U(\text{Mn}) = 5\text{eV}$  is used [10–14]. However, previous studies only considered nonmagnetic [14] or ferromagnetic [10–12] configurations, while  $\text{Li}_2\text{MnO}_3$  is antiferromagnetic with  $T_N = 36\text{K}$  in the experiment [8]. Given that the spin state of single transition metal (TM) ion and their magnetic interactions can strongly depend on  $U$ , systematic study is needed within DFT+ $U$ . In Section III A, we show that  $U(\text{Mn}) = 2$  is needed to obtain the proper magnetic ground state. While the antiferromagnetic ground state can be obtained by DFT+ $U$ , the paramagnetic phase of  $\text{Li}_2\text{MnO}_3$  cannot be described within DFT+ $U$ . Studying the paramagnetic phase is essential, since the operating temperature of the battery is around 300 K. In Section III B, we systematically study the electronic structure of paramagnetic phase within DFT+DMFT.

### A. DFT+U

We begin the discussion by studying the magnetic phase of  $\text{Li}_2\text{MnO}_3$ .  $\text{Li}_2\text{MnO}_3$  is antiferromagnetic with Neel temperature of  $T_N = 36$  K, and the magnetic propagation vector is  $Q_m = (0, 0, 0.5)$  [9]. Among the possible magnetic configuration with  $Q_m = (0, 0, 0.5)$ ,  $\Gamma_{3g}$  [9] and  $\Gamma_{2u}$  [8] are suggested as the ground state, and the recent powder neutron diffraction data and single crystal neutron diffraction data at 6 K showed that the ground state is  $\Gamma_{2u}$ . Magnetic moment of Mn is  $2.3\text{--}2.7 \mu_B$  [8, 9], indicating that Mn has high-spin state.

In Figure 3, we compare the energies of the ferromagnetic (FM), antiferromagnetic  $\Gamma_{3g}$  and  $\Gamma_{2u}$  phases.  $\Gamma_{2u}$  phase is most stable if  $U(\text{Mn}) \leq 2$ , while  $\Gamma_{3g}$  becomes more stable when  $U(\text{Mn}) > 2$ , while Mn ion always has the high-spin state. This result shows that  $U(\text{Mn}) \leq 2$  is needed to obtain the experimental ground state. Previous linear response calculation for spinel  $\text{Mn}^{4+}$  suggested that  $U(\text{Mn}) = 5.04$  eV [31], and many DFT+ $U$  studies [10–14] used  $U(\text{Mn}) = 5$  eV based on this study. We note that using  $U$  values from the linear response theory within GGA+ $U$  overestimate the correlation in the transition metal oxides, such as nickelates, and the overestimation can be fixed within DMFT [32]. Therefore, we suggest that within DFT+ $U$ ,  $U(\text{Mn}) = 2$  eV is reasonable value to study the electronic and magnetic properties of  $\text{Li}_2\text{MnO}_3$ . The energy difference between  $\Gamma_{2u}$  and other magnetic configuration decreases as a function of  $U$ . With  $U(\text{Mn}) = 2$  eV,  $\Gamma_{2u}$  is more stable than FM and  $\Gamma_{3g}$  by 1.8 and 0.8 meV, respectively, consistent with the low  $T_N = 36$  K. Magnetic moment of Mn in  $\Gamma_{2u}$  phase is  $2.8 \mu_B$ , similar to the experimental value  $2.3 \mu_B$ .

Next we study the effect of  $U$  on the electronic structure and energy gap of  $\text{Li}_2\text{MnO}_3$ . Mn ion in  $\text{Li}_2\text{MnO}_3$  has  $4+$  charge state with 3  $d$  electrons, and it has high-spin state.  $\text{MnO}_6$  in  $C2/m$  phase has  $C_{2h}$  point group symmetry, which splits the  $d$  bands into 3 low  $A$  bands ( $d_{xy}$ ,  $d_{z^2}$ , and  $d_{x^2-y^2}$ ) and 2 high  $B$  bands ( $d_{xz}$  and  $d_{yz}$ ). In the high-spin state, 3 electrons of Mn occupy the three spin-up  $A$  bands (see Figure 8 in Appendix). Therefore, there are two types of splittings which determine the energy gap ( $E_g$ ): (i) crystal field splitting ( $\Delta_{\text{CF}}$ ) between  $A$  and  $B$  bands, and (ii) exchange splitting ( $\Delta_{\text{ex}}$ ) between spin-up  $A$  and spin-down  $A$  bands. These splittings are also presented in the projected density of states in Fig. 4.

For the non spin-polarized phase with  $U(\text{Mn}) = 0$ ,  $\Delta_{\text{CF}}$  is around 2.5 eV while  $\Delta_{\text{ex}}$  is only  $\sim 0.6$  eV. As a result,  $E_g$  is almost zero, as shown in Fig. 4(a). If the spin-polarization is turned on [Fig. 4(b)], then  $\Delta_{\text{ex}}$  is dramatically enhanced to  $\sim 2.2$  eV, and  $\Delta_{\text{CF}}$  is also increased to  $\sim 3$  eV.  $\Delta_{\text{ex}}$  determines the size of the energy gap since  $\Delta_{\text{ex}} < \Delta_{\text{CF}}$ , and the  $E_g$  becomes 1.19 eV. If nonzero  $U$  is applied, then both  $\Delta_{\text{ex}}$  and  $\Delta_{\text{CF}}$  are increased, as shown in Fig. 4(c). With  $U(\text{Mn}) = 2$ , we obtain  $E_g = 2.0$  eV, similar to the experimental gap  $2.1\text{--}2.17$  eV [6, 7]. When  $U(\text{Mn}) = 5$ ,  $E_g$  is 1.9 eV, similar to the value with  $U(\text{Mn})$

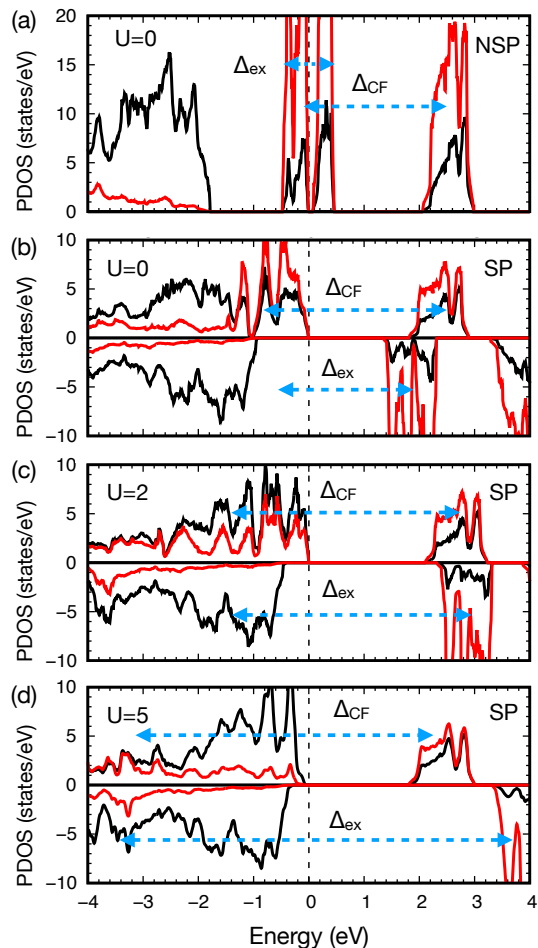


FIG. 4: Projected density of states (PDOS) onto the Mn  $d$  (red) and O  $p$  (black) in  $\text{Li}_2\text{MnO}_3$ . (a)  $U(\text{Mn}) = 0$  for non spin-polarized configuration, (b)  $U(\text{Mn}) = 0$  for spin-polarized configuration (ferromagnetic), (c)  $U(\text{Mn}) = 2$  and (d)  $U(\text{Mn}) = 5$  for spin-polarized configuration.

$= 2$ . While the occupied Mn  $d$  band is lowered with large  $U$ , the energy of the valence band maximum is less sensitive to  $U$ , and thus  $E_g$  does not change much.

### B. DFT+DMFT

As mentioned,  $\text{MnO}_6$  has  $C2/m$  point group symmetry, which is different from the cubic ( $O_h$ ) symmetry (See Appendix A). In the cubic ( $O_h$ ) phase, the local Mn–O coordinates and the global coordinates based on the symmetry are parallel, thus the Hamiltonian based on the  $d$  orbital does not have off-diagonal terms. On the other hand, in the  $C2/m$  phase, local Mn–O axes and the global axes are not parallel. Crystal splitting of  $d$  bands shown in Fig. 8(b) is based on the global axes, not the local axes. Therefore, if we use the global coordinates for the Wannier projection, there are large off-diagonal terms:

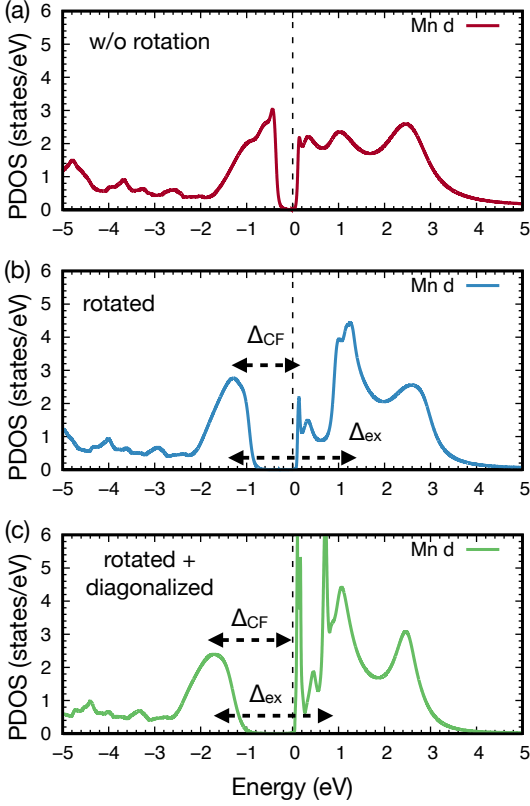


FIG. 5: DFT+DMFT spectral functions of Mn  $d$  Wannier orbitals. (a) global coordinate is used for Wannier projection, (b) local coordinate obtained by unitary rotation matrix is used for Wannier projection, and (c) block diagonal part of Mn  $d$  Hamiltonian is diagonalized. The calculations use  $U = 5$  eV,  $J = 0.9$  eV, and a temperature of 300 K.

$$\mathbf{H}_i = \begin{matrix} & d_{z^2} & d_{xz} & d_{yz} & d_{x^2-y^2} & d_{xy} \\ \begin{matrix} d_{z^2} \\ d_{x^2-y^2} \\ d_{yz} \\ d_{x^2-y^2} \\ d_{xy} \end{matrix} & \begin{pmatrix} 3.784 & 0.002 & 0 & -0.007 & 0 \\ 0.002 & 4.583 & 0 & \mathbf{-0.592} & 0 \\ 0 & 0 & 4.578 & 0 & \mathbf{0.584} \\ -0.007 & \mathbf{-0.592} & 0 & 4.153 & 0 \\ 0 & 0 & \mathbf{0.584} & 0 & 4.152 \end{pmatrix} \end{matrix} \quad (3)$$

Using the non-rotated Hamiltonian, we employed DFT+DMFT calculations plot the spectral functions in Fig. 5(a). Since the battery is used at room temperature, we use the temperature of 300 K, and consider the paramagnetic phase since  $T_N = 65$  K is much lower than 300 K. Using the non-rotated basis within DMFT,  $E_g$  is only 0.4 eV, much smaller than the experimental value.

Since the large off-diagonal terms give large error of the energy gap, we also use the local coordinate by applying the unitary rotation matrix to the Hamiltonian, which gives the minimum values of the off-diagonal terms. As

shown in Eq. 4,

$$\mathbf{H}_{rot} = \begin{matrix} & d_{z^2} & d_{xz} & d_{yz} & d_{x^2-y^2} & d_{xy} \\ \begin{matrix} d_{z^2} \\ d_{xz} \\ d_{yx} \\ d_{x^2-y^2} \\ d_{xy} \end{matrix} & \begin{pmatrix} 4.069 & 0.018 & -0.009 & \mathbf{-0.530} & 0.059 \\ 0.018 & 3.775 & 0.064 & 0.010 & 0.003 \\ -0.009 & 0.064 & 4.997 & -0.011 & 0.006 \\ \mathbf{-0.530} & 0.010 & -0.011 & 4.668 & -0.101 \\ 0.059 & 0.003 & 0.006 & -0.101 & 3.754 \end{pmatrix} \end{matrix} \quad (4)$$

off-diagonal terms are much smaller, and  $E_g$  is increased to 0.6 eV. However,  $E_g$  is still much smaller the experimental gap. As shown in Fig. 5(b), underestimation of  $E_g$  is due to the small  $\Delta_{CF}$ .  $\Delta_{CF}$  within DMFT with rotated Wannier axes is around 1.5 eV, which is much smaller than the value within DFT+ $U$  ( $\sim 3$  eV). On the other hand,  $\Delta_{ex}$  is around 2.7 eV, does not affect to  $E_g$ .

To resolve the underestimation of  $E_g$  within DFT+DMFT, we diagonalize the each Mn  $d$  block of the Hamiltonian (orange boxes in Fig. 2), which can be obtained by the unitary rotation matrix. As presented in Fig. 5(b),  $E_g$  within DMFT is increased to 0.8 eV. Using the diagonalized Hamiltonian, we also consider various  $U$  and double counting parameter  $\alpha$  (see Eq. 2). Interestingly,  $\Delta_{CF}$  and resulted  $E_g$  are sensitive on  $U$ . As shown in Fig. 6,  $E_g$  with  $U=5$  and 7 are 0.8 and 0.9eV, respectively.

On the other hand,  $\Delta_{CF}$  and resulted  $E_g$  are more sensitive to  $\alpha$ . With  $U=5$ ,  $E_g$  is increased to 1.4 eV when  $\alpha=0.8$ . In addition, when  $\alpha=0.8$ , increasing  $U=5$  to 7 enhances  $E_g$  from 1.4 to 2.0 eV. The different  $\alpha$  values effectively shift the energy of the  $d$  bands,  $p-d$  covalency can be tuned by  $\alpha$ , since the energy of the  $d$  bands is effectively shifted by different  $\alpha$  values. Therefore,  $E_g$  sensitive on  $\alpha$  indicate that  $p-d$  correlation  $U_{pd}$  is important on  $\Delta_{CF}$ , and changing  $U(\text{Mn})$  for the  $pd$  model Hamiltonian is not enough since it only changes the  $d-d$  correlation.

In this reason, we also consider the  $d$ -only model Hamiltonian to describe the electronic structure of  $\text{Li}_2\text{MnO}_3$ . While the Wannier  $d$  orbitals are close to the Mn  $d$  orbital in the  $pd$  model, Wannier  $d$  orbitals in  $d$ -only model are the hybridized Mn  $d$  and O  $p$  orbitals. Thus, the effect of  $U(\text{Mn})$  on  $d$ -only Wannier Hamiltonian is similar to the effects of applying both  $U_{dd}$  and  $U_{pd}$  to the  $pd$  model Hamiltonian. Therefore,  $\Delta_{CF}$  and  $E_g$  are sensitive to  $U(\text{Mn})$  within the  $d$ -only model. Indeed, the value of  $E_g$  is similar to  $U(\text{Mn})$  using  $d$ -only Hamiltonian within DMFT. With  $U(\text{Mn}) = 2.2$  eV, we obtain  $E_g = 2.1$  eV, as presented in Fig. 7.



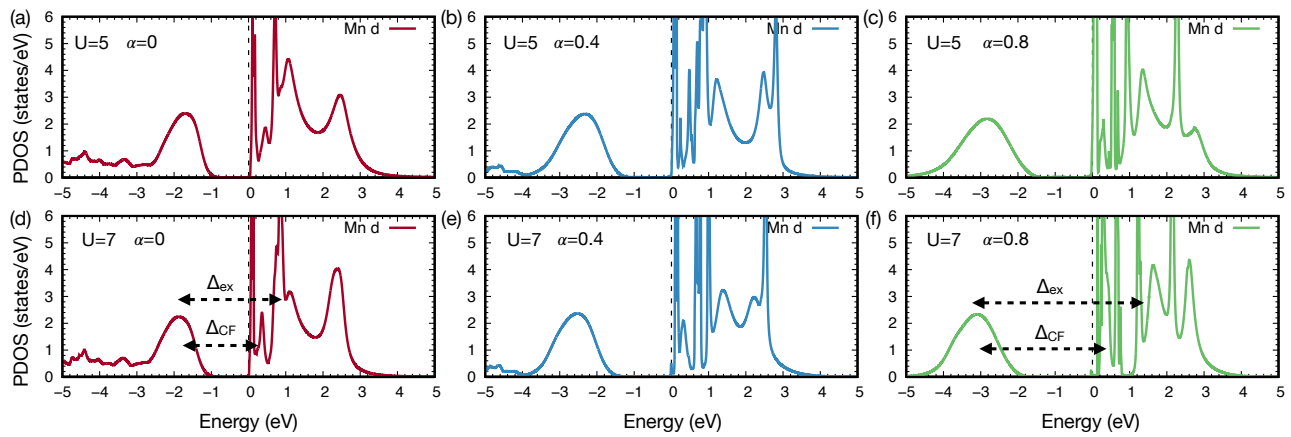


FIG. 6: DFT+DMFT spectral functions of Mn  $d$  Wannier orbitals with different  $U$  and  $\alpha$ . The calculations use temperature of 300 K.

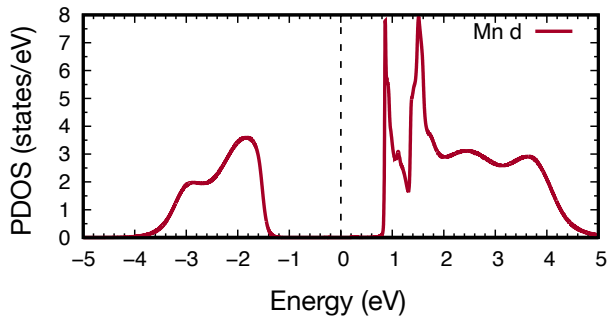


FIG. 7: DFT+DMFT spectral functions of Mn  $d$  Wannier orbitals with  $d$ -only model. The calculations use  $U = 2.2$  eV,  $J = 0.9$  eV, and a temperature of 300 K.

#### IV. Summary

In this work, we show that the off-diagonal terms of Mn  $d$  Hamiltonian and  $p$ - $d$  interaction play crucial role on the electronic structure of  $\text{Li}_2\text{MnO}_3$ , through DFT+DMFT calculations. We show that when only the diagonal terms are treated in the CTQMC solver to avoid the sign problem, the off-diagonal terms of the Mn  $d$  block of the Wannier Hamiltonian play an important role in the electronic structure. Due to the monoclinic symmetry ( $C2/m$ ) of  $\text{Li}_2\text{MnO}_3$ , the off-diagonal terms of Mn  $d$  are large if the global coordinate is chosen, and thus the energy gap is greatly suppressed compared to the experimental value. Choosing local coordinate can reduce the magnitude of the off-diagonal terms and increase the band gap enormously, but it is much smaller than the experimental value.

Therefore, we diagonalize the Mn  $d$  block of the Wannier Hamiltonian by multiplying the unitary rotation matrix, and show that the energy gap is further enhanced, while the gap is still not large enough. We find that

since Mn  $d$  - O  $p$  hybridization is strong, increasing  $U_{dd}$  is not enough, and applying  $p$ - $d$  correlation by changing the double counting parameter is essential to obtain the experimental gap. To verify this idea, we also consider  $d$ -only model Hamiltonian, since the basis of the  $d$ -only model is hybridized state of Mn  $d$  and O  $p$ . We confirm that energy gap is sensitive on  $U$ , indicating that both  $dd$  and  $pd$  correlations are important on the electronic structure of  $\text{Li}_2\text{MnO}_3$ .

We also show that the magnetic ground state strongly depend on  $U$ . While the antiferromagnetic states ( $\Gamma_{2u}$  or  $\Gamma_{3g}$ ) are more stable than the ferromagnetic state in the wide range of  $U$  ( $U \leq 5$ ), experimentally observed ground state  $\Gamma_{2u}$  phase is most stable with  $U \leq 2$ . Therefore, we suggest that the careful choice of  $U$  is needed for future DFT+ $U$  studies of  $\text{Li}_2\text{MnO}_3$ .

## V. Acknowledgments

This research is supported by the Vehicle Technologies Office (VTO), Department of Energy (DOE), USA, through the Battery Materials Research (BMR) program. We also acknowledge financial support from the U.S.

Department of Energy, Office of Science, Office of Basic Energy Sciences, Materials Science and Engineering Division. We gratefully acknowledge the computing resources provided on Bebop, a high-performance computing cluster operated by the Laboratory Computing Resource Center at the Argonne National Laboratory.

- 
- [1] J. B. Goodenough and K.-S. Park, *Journal of the American Chemical Society* **135**, 1167 (2013), pMID: 23294028, <https://doi.org/10.1021/ja3091438>, URL <https://doi.org/10.1021/ja3091438>.
- [2] D.-H. Seo, J. Lee, A. Urban, R. Malik, S. Kang, and G. Ceder, *Nature Chemistry* **8**, 692 (2016), URL <https://doi.org/10.1038/nchem.2524>.
- [3] M. Sathiya, G. Rousse, K. Ramesha, C. P. Laisa, H. Vezin, M. T. Sougrati, M.-L. Doublet, D. Foix, D. Gonbeau, W. Walker, et al., *Nature Materials* **12**, 827 (2013), ISSN 1476-4660, number: 9 Publisher: Nature Publishing Group, URL <https://www.nature.com/articles/nmat3699>.
- [4] J. Lee, A. Urban, X. Li, D. Su, G. Hautier, and G. Ceder, *Science* **343**, 519 (2014), <https://www.science.org/doi/pdf/10.1126/science.1246432>, URL <https://www.science.org/doi/abs/10.1126/science.1246432>.
- [5] N. Yabuuchi, K. Yoshii, S.-T. Myung, I. Nakai, and S. Komaba, *Journal of the American Chemical Society* **133**, 4404 (2011), pMID: 21375288, <https://doi.org/10.1021/ja108588y>, URL <https://doi.org/10.1021/ja108588y>.
- [6] S. Tamilarasan, S. Laha, S. Natarajan, and J. Gopalakrishnan, *J. Mater. Chem. C* **3**, 4794 (2015), URL <http://dx.doi.org/10.1039/C5TC00616C>.
- [7] B. Singh and P. Singh, *SN Applied Sciences* **2**, 506 (2020), ISSN 2523-3971, URL <https://doi.org/10.1007/s42452-020-2260-z>.
- [8] S. Lee, S. Choi, J. Kim, H. Sim, C. Won, S. Lee, S. A. Kim, N. Hur, and J.-G. Park, *Journal of Physics: Condensed Matter* **24**, 456004 (2012), URL <https://dx.doi.org/10.1088/0953-8984/24/45/456004>.
- [9] P. Strobel and B. Lambert-Andron, *Journal of Solid State Chemistry* **75**, 90 (1988), ISSN 0022-4596, URL <https://www.sciencedirect.com/science/article/pii/0022459688903052>.
- [10] R. Xiao, H. Li, and L. Chen, *Chemistry of Materials* **24**, 4242 (2012), URL <https://doi.org/10.1021/cm3027219>.
- [11] S. Wang, J. Liu, and Q. Sun, *J. Mater. Chem. A* **5**, 16936 (2017), URL <http://dx.doi.org/10.1039/C7TA04941B>.
- [12] H. Chen and M. S. Islam, *Chemistry of Materials* **28**, 6656 (2016), URL <https://doi.org/10.1021/acs.chemmater.6b02870>.
- [13] Z. Chen, J. Li, and X. C. Zeng, *Journal of the American Chemical Society* **141**, 10751 (2019), pMID: 31251049, <https://doi.org/10.1021/jacs.9b03710>, URL <https://doi.org/10.1021/jacs.9b03710>.
- [14] K. Hikima, K. Shimizu, H. Kiuchi, Y. Hinuma, K. Suzuki, M. Hirayama, E. Matsubara, and R. Kanno, *Journal of the American Chemical Society* **144**, 236 (2022), pMID: 34957828, <https://doi.org/10.1021/jacs.1c09087>, URL <https://doi.org/10.1021/jacs.1c09087>.
- [15] E. B. Isaacs and C. A. Marianetti, *Phys. Rev. B* **102**, 045146 (2020), URL <https://link.aps.org/doi/10.1103/PhysRevB.102.045146>.
- [16] D. M. Korotin, D. Novoselov, and V. I. Anisimov, *Phys. Rev. B* **99**, 045106 (2019), URL <https://link.aps.org/doi/10.1103/PhysRevB.99.045106>.
- [17] V. Singh, U. Herath, B. Wah, X. Liao, A. H. Romero, and H. Park, *Computer Physics Communications* **261**, 107778 (2021), ISSN 0010-4655, URL <http://www.sciencedirect.com/science/article/pii/S001046552030388X>.
- [18] H. Park, R. Nanguneri, and A. T. Ngo, *Phys. Rev. B* **101**, 195125 (2020), URL <https://link.aps.org/doi/10.1103/PhysRevB.101.195125>.
- [19] P. E. Blöchl, *Phys. Rev. B* **50**, 17953 (1994), URL <http://link.aps.org/doi/10.1103/PhysRevB.50.17953>.
- [20] J. P. Perdew, A. Ruzsinszky, G. I. Csonka, O. A. Vydrov, G. E. Scuseria, L. A. Constantin, X. Zhou, and K. Burke, *Phys. Rev. Lett.* **100**, 136406 (2008), URL <http://link.aps.org/doi/10.1103/PhysRevLett.100.136406>.
- [21] G. Kresse and D. Joubert, *Phys. Rev. B* **59**, 1758 (1999), URL <http://link.aps.org/doi/10.1103/PhysRevB.59.1758>.
- [22] N. Marzari, A. A. Mostofi, J. R. Yates, I. Souza, and D. Vanderbilt, *Rev. Mod. Phys.* **84**, 1419 (2012), URL <https://link.aps.org/doi/10.1103/RevModPhys.84.1419>.
- [23] K. Haule, *Phys. Rev. B* **75**, 155113 (2007), URL <https://link.aps.org/doi/10.1103/PhysRevB.75.155113>.
- [24] E. Gull, A. J. Millis, A. I. Lichtenstein, A. N. Rubtsov, M. Troyer, and P. Werner, *Rev. Mod. Phys.* **83**, 349 (2011), URL <https://link.aps.org/doi/10.1103/RevModPhys.83.349>.
- [25] A. I. Lichtenstein, V. I. Anisimov, and J. Zaanen, *Phys. Rev. B* **52**, R5467 (1995), URL <http://link.aps.org/doi/10.1103/PhysRevB.52.R5467>.
- [26] H. Park, A. J. Millis, and C. A. Marianetti, *Phys. Rev. B* **92**, 035146 (2015), URL <http://link.aps.org/doi/10.1103/PhysRevB.92.035146>.
- [27] H. Park, A. J. Millis, and C. A. Marianetti, *Phys. Rev. Lett.* **109**, 156402 (2012), URL <https://link.aps.org/doi/10.1103/PhysRevLett.109.156402>.
- [28] V. I. Anisimov, J. Zaanen, and O. K. Andersen, *Phys. Rev. B* **44**, 943 (1991), URL <https://link.aps.org/doi/10.1103/PhysRevB.44.943>.
- [29] J. Chen, A. J. Millis, and C. A. Marianetti, *Phys. Rev. B* **91**, 241111 (2015), URL <http://link.aps.org/doi/10.1103/PhysRevB.91.241111>.
- [30] H. Chen and A. J. Millis, *Physical Review B* **93**, 045133 (2016), URL <https://link.aps.org/doi/10.1103/PhysRevB.93.045133>.
- [31] F. Zhou, M. Cococcioni, C. A. Marianetti, D. Mor-

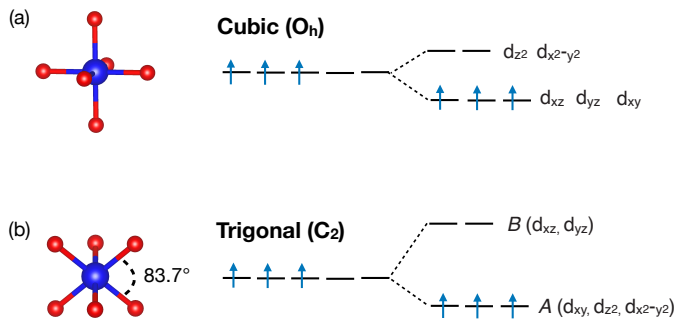


FIG. 8: Schematic band splitting based on the (a) cubic ( $O_h$ ) and (b) trigonal ( $C_{2v}$ ) crystal fields.

- gan, and G. Ceder, Phys. Rev. B **70**, 235121 (2004), URL <https://link.aps.org/doi/10.1103/PhysRevB.70.235121>.
- [32] H. Park, A. J. Millis, and C. A. Marianetti, Phys. Rev. B **90**, 235103 (2014), URL <https://link.aps.org/doi/10.1103/PhysRevB.90.235103>.

### A. Crystal symmetry of $\text{Li}_2\text{MnO}_3$

In Figure 8 we present the atomic structure with cubic and trigonal symmetries, and schematic band pictures.